N93-29364

HYPERVELOCITY IMPACT SURVIVABILITY EXPERIMENTS FOR CARBONACEOUS IMPACTORS

T. E. Bunch
NASA Ames Research Center
Moffett Field, CA 94035-1000

Luann Becker and Jeffrey Bada
Scripps Institute of Oceanography
University of California at San Diego, La Jolla, CA 92093

John Macklin
Department of Chemistry
University of Washington, Seattle, WA 98195

Filippo Radicati di Brozolo and R. H. Fleming
Charles Evans and Associates
301 Chesapeake Drive, Redwood City, CA 94063

Jozef Erlichman
TMA/Norcal
2030 Wright Ave., Richmond, CA 94804

ABSTRACT

We performed a series of hypervelocity impact experiments using carbon-bearing impactors (diamond, graphite, fullerenes, phthalic acid crystals, and Murchison meteorite) into Al plate at velocities between 4.2 and 6.1 km sec^{-1}. These tests were made in order to (a) determine the survivability of carbon forms and organic molecules in low hypervelocity impact, (b) characterize carbonaceous impactor residues, and (c) determine whether or not fullerenes could form from carbonaceous impactors, under our experimental conditions, or survive as impactors.

An analytical protocol of field emission SEM imagery, SEM-EDX, laser Raman spectroscopy, single and 2-stage laser mass spectrometry, and laser induced fluorescence (LIF) found that : (1) diamonds did not survive impact at 4.8 km sec^{-1}, but were transformed into various forms of disordered graphite, (2) intact, well-ordered graphite impactors did survive impact at 5.9 km sec^{-1}, but were only found in the crater bottom centers; the degree of impact-induced disorder in the graphite increases outward (walls, rims, ejecta), (3) phthalic acid crystals were destroyed on impact (at 4.2 km sec^{-1}), although a large proportion of phthalic acid molecules did survive impact, (4) fullerenes did not form as products of carbonaceous impactors (5.9-6.1 km sec^{-1}); fullerene impactor molecules mostly survived impact at 5.9 km sec^{-1} and, (5) two Murchison meteorite samples (launched at 4.8 and 5.9 km sec^{-1}) show preservation of some higher mass polycyclic aromatic hydrocarbons (PAHs) compared with the non-impacted sample. Each impactor type shows unique impactor residue morphologies produced at a given impact velocity.

An expanded methodology is presented to announce relatively new analytical techniques together with innovative modifications to other methods that can be used to characterize small impact residues in LDEF craters, in addition to other acquired extraterrestrial samples.

INTRODUCTION

Observations of LDEF impact craters indicate that a small but unknown fraction of the craters contain dark residues, possibly carbon-bearing (e. g., refs. 1 and 2). Few detailed investigations of carbonaceous impactors have been made (e. g., ref. 3); however, the information contained within carbonaceous impactors is vital to understanding their origin and significance. Information on the behavior of carbonaceous materials on impact is virtually unknown, although Peterson *et al.*, 1991 (ref. 4) have performed shock experiments on amino acid survivability. Two of the three crystalline forms of carbon, diamond and graphite, are known to occur in meteorites (ref. 5) and diamond occurs in the interstellar medium (ISM) (ref. 6). Amorphous carbon and poorly crystallized graphite (PCG) in carbonaceous chondrites forms the bulk of their carbon inventories together with many organic compounds including polycyclic aromatic hydrocarbons (PAHs) which are also found in the ISM (ref. 7). These and other organic compounds may occur in comets (e. g., ref. 8). The possibility exists that LDEF sampled carbonaceous-bearing particles from all of these environments. In addition, fullerene, the third form of carbon, was recently found in an LDEF crater using single laser ionization mass spectrometry (ref. 9), although fullerenes have not yet been identified in meteorites or in the ISM.

In attempting to characterize and interpret LDEF carbonaceous residues, several first -order questions should be addressed: 1) Can carbon crystalline phases and organic compounds survive low velocity (< 6 km sec^{-1}) impact and if they do survive, what are their characteristics? 2) If they do not survive impact, what are their impact products? 3) Were the fullerenes made by impact from other carbonaceous materials or were they primary and survived impact? Light gas gun hypervelocity experiments were conducted in order to possibly constrain, within our experimental capabilities, these and other issues in addition to testing techniques and establishing characteristic impactor criteria.

In an attempt to achieve some of our stated goals, we used two relatively new analytical techniques that have exceptionally low detection limits for carbonaceous materials in very small particles. The survivability of PAHs and other carbonaceous materials in impacted Murchison meteorite was tested using laser desorption/laser ionization mass spectrometry techniques (2-stage laser mass spectrometry). At best, the detection limits for this technique are probably in the ppm to sub-ppm range. Although this sensitivity is adequate for the detection of PAHs, enhanced sensitivity may be necessary to determine whether or not other carbonaceous materials, e. g., fullerenes, are present in our test samples. By using laser induced fluorescence (LIF), 10^{-11}g or about 10^{-14} moles of C_{60} can be detected, which allows for the detection of C_{60} on the sub ppb level for a gram of sample (ref. 10).

We report here some of the preliminary results of morphological, compositional, and structural studies made on carbon and carbonaceous-bearing experimentally-formed impact residues.

SAMPLE SELECTION, EXPERIMENTAL AND ANALYTICAL TECHNIQUES

Sample Selection and Experimental Conditions

For the purposes of this study, the three forms of crystalline carbon (diamond, submicron graphite, coarse-grained graphite, fullerenes), Murchison carbonaceous chondrite and solid phthalic acid particles were chosen for impact experiments.The carbon forms were used to test the hypothesis that fullerenes may either form from graphite or diamond on impact, or that fullerenes are stable on impact at ≈ 6 km sec^{-1} and therefore preexisted before encountering LDEF (see ref. 9). Murchison was used to simulate carbonaceous meteorite impactors and solid phthalic acid was impacted to extend the impact survivability range initiated in an earlier study (ref. 3).

Submicron graphite, coarse-grained graphite, and fullerenes were accelerated into Al targets at 6.1, 5.92, and 5.89 km sec^{-1}, respectively; Murchison particles at 4.8 and 5.89 km sec^{-1} ;

diamond at 4.8 km sec^{-1}, and phthalic acid at 4.23 km sec^{-1}. The prelaunch impactor particle size for Murchison, coarse graphite, and phthalic acid was ≈ 0.2 mm (minimum diameter), diamond ≈ 0.3-0.4 mm, fullerenes ≈ 0.03-0.06 mm, and submicron graphite was < one micron but electrostatically attracted particle clumps as large as 0.1 mm were noted. For experiments of this type, the Ames light gas gun is limited to acceleration velocities of < 6.3 km sec^{-1}. Peak pressures and temperatures cannot be directly measured.

Experimental Methodology

Two-stage Light Gas Gun Experiments

Projectile grains were loaded into a small (3 mm cavity) Al carrier cup (Fig. 1a), capped with an Al plate and fitted into a sabot for launching (Fig. 1b). The two-stage light gas gun accelerates the sabot down a rifled barrel (1.2 m long; bore dia = 9 mm) to velocities of ≈ 2-6.5 km sec^{-1} depending on the amount of the powder charge (first stage), which in turn determines the speed of the deformable ram that compresses hydrogen gas (second stage). When the gas reaches a certain critical pressure, a diaphram ruptures and the gas propels the sabot down the barrel. At the end of the barrel, the sabot, carrier, and particles are separated in a "blast" chamber, particle velocities are electronically recorded, the in-flight particles are photographed, and the particles continue on to impact with the target plate (at 90°to the target) in an evacuated chamber (vacuum pressures nominally <1 mm of Hg). The impacted plate also serves as a witness plate (Fig. 1c) which has a 2.5 cm dia hole through which the carrier travels. This technique allows only particles to impact, the alignment of the launch can be measured, and the range in diameters of the launched particles at the impact point can be measured from the holes in the mylar covering which is attached beneath the hole (Fig. 1c). This cluster shot approach is necessary for projectiles < 1.0 mm in diameter as smaller grains cannot be individually launched.

Observational and Analytical

Observational

Samples were dry cut from the target plate. Craters and retained impactor debris were first observed by an optical light microscope, then by field emission scanning electron microscopy (FESEM). Samples were then submitted to the analytical protocol given below.

Analytical

Micro RAMAN Spectroscopy. Raman spectra were obtained by using the 488.0 nm line of a coherent radiation Innova 90 argon ion laser. The power of the laser radiation used here was between 20 and 40 mW and focused to a spot size of 5 microns. The scattered radiation was dispersed with a SPEX Industries 1477B Triplemate spectrometer equipped with a SPEX Micromate microsampling system that includes a modified Zeiss microscope and detected by a Reticon intensified diode array. The spectrometer slitwidth was kept at 300 microns. Integration times on the diode array ranged from 5 to 10 seconds and 10 or 20 acquisitions were averaged before data collection. Data acquisition and storage were accomplished by a PC computer system.

Single Stage Laser Ionization Mass Spectrometry (LIMS). Principles and applications of this methodology are described in Ref. (11). The fourth harmonic of a Nd:YAG laser (266nm; 1.0-1.5mJ/pulse; 50 to 10 nsec pulse width; 2.5 Hz repetition rate) is used to produce desorption and ionization of species at the sample surface. The strong selectivity in favor of low ionization

potential elemental signals (e. g., alkalis) or fullerenes, which have a strong absorption band in the UV at 264 nm (ref. 12), suggests that Resonance Enhanced Multiphoton Ionization (REMPI) is present under these conditions. The ions are mass separated in a reflector type time-of-flight (mass resolution = 450 at m/z 41), and detected with a 17 stage electron multiplier (Thorn-EMI). The data presented are the sum of typically 150 to 200 laser shots.

Laser Ionization Mass Spectrometry (L^2MS). The two-step laser methodology has been described elsewhere (ref. 13). In the first step, the pulsed output of a CO_2 laser (10.6 um; 20 mJ/pulse; 10 u-sec pulse width; 5-Hz repetition rate) is focused onto a small stainless steel disk (~1mm diameter) containing the meteorite sample. The infrared (IR) radiation is readily absorbed by the meteorite minerals and causes the ejection of intact neutral molecules from their surfaces in a rapid, laser-induced thermal desorption process. The fact that desorption dominates over decomposition in rapid laser heating processes is well documented (refs.13, 14). The sample can be rotated manually in order to expose fresh surface to the desorption laser. After an appropriate time delay (~130 usec), the fourth harmonic of a Nd:YAG laser (266 nm; 1.5-2.0 mJ/pulse; 10-nsec pulse width; 5-Hz repetition rate) is used to induce 1+1 resonance-enhanced multiphoton ionization (REMPI) of the desorbed molecules in an interaction region about 5mm from the surface. REMPI causes soft ionization so that the parent ions of the desorbed aromatic compounds almost exclusively dominate the spectrum. Total ionization efficiency is about a factor of 100 to 1000 greater than that of methods where ions are directly produced on a surface. One of the advantages to the L^2MS system is the spatial and temporal separation of the desorption and ionization which results in more control than in one-step desorption /ionization processes. The laser-generated ions are mass separated in a linear TOF system (mass resolution = 500) and detected with a microchannel plate array. Data for the meteorite samples were averaged over 100 laser shots, although a complete mass spectrum can be obtained from a single shot.

Samples were prepared using MALDI (matrix assisted laser desorption ionization). Previous reports have shown that laser desorption of neutral molecules can be improved by spraying a fine layer of sample on top of a matrix that absorbs at the wavelength of the laser (ref. 15). For our L^2MS system, the organic substrate sinapinic acid was used as the matrix. The matrix is sprayed directly onto the stainless steel disc (100 ng/mm^2) insuring that the substrate is evenly dispersed over the entire surface of the disc. The impacted meteorite sample (sonicated in toluene) is then sprayed on top of the sinapinic acid film. The sample disc is mounted on a 7-mm diameter teflon probe tip and is introduced to the TOF mass spectrometer through a separate antechamber pumped down to zero millitorr before introducing it to the high vacuum (10^{-7} torr) of the system. Sample introduction takes about 2 minutes and the spectrum can be recorded immediately thereafter.

Laser Induced Fluorescence (LIF). The development of LIF has provided a highly sensitive method for the detection of a variety of fluorescent molecules (ref. 16), especially those which exhibit weak fluorescence. The LIF system has been described elsewhere (ref. 17) and uses a 325 nm beam of a He-Cd laser focused into a 0.1 mm fused silica optic fiber which transports the excitation light into a 200 micron ID deactivated fused silica capillary column. The flow-through-cell, which was made by carefully removing about 0.5 cm of the polyimide coating on the fused silica column, has a volume of about 100 nl. The emission radiation is collected using two 0.6 mm fused silica optic fibers positioned at right angles to the excitation beam, passed through a 370 nm high pass cutoff filter, delivered to a monochromator set at 400 nm with a 10 nm exit slit, and detected with a photomultiplier. Toluene was used for column elution and was delivered to the capillary column by an HPLC pump. Samples containing various concentrations of Murchison meteorite in toluene were introduced into the capillary column with an injection valve fitted with a 100 microliter sample loop.

RESULTS

Crater and Impactor Residue Characteristics

Microscopic, FESEM, and Raman Characteristics

General. Figures 2 through 10 show microcsopic and FESEM images of the experimentally produced craters, in addition to one LIMS spectrum. Submicron graphite, graphite, and diamond craters show an increase in the presence of dark impactor crater liners from low amounts (Fig. 2a) to relatively high amounts of dark, thick liners (diamond: Fig. 5). Fullerene craters (Fig. 7) are similar to graphite craters (Fig. 4) in the amounts of visible, dark impactor residue, although the residue color is dark, purple-red which is the same as the unlaunched fullerenes. Phthalic acid craters are mostly clear with little visible dark residue; Murchison craters look very similar to graphite craters in terms of crater morphology and amount of impactor residue. Only the diamond craters show significant ejecta or particulate fall-out around the outside of the craters.

Crater diameters show considerable range for all experiments. For example, whereas diamond craters are mostly 1-1.3 mm in dia, some are as small as 0.01mm. Two factors are mostly responsible for the large variations in crater size: (1) break-down of a particle along zones of structural weaknesses during acceleration and/or (2) in-flight, mid-range collisions. In addition, observations of prelaunch submicron graphite projectiles indicate that they consisted of variable size lumps (microns to tens of microns) of electrostatically attracted submicron grains.

Graphite, diamond, fullerene, and Murchison craters tend to be round in shape with depth to diameter ratios (P/D_c) of between 0.55 and 0.8. Phthalic acid craters (Fig. 8) are irregular in shape and are shallower, on the average, than other craters ($P/D_c = 0.45$). The large oval submicron graphite crater in Fig. 2 has a P/D_c of only 0.4; all other submicron graphite craters are < 0.1 mm in dia and have a P/D_c of 0.45 - 0.55.

Submicron graphite Craters. Our original intent was to launch amorphous carbon as one of the impactors. However, Raman analysis of the commercially obtained prelaunched "amorphous" carbon shows that it is not amorphous and matches the characteristics of well-ordered graphite. Therefore, instead of having craters formed by graphite and amorphous carbon, we have craters formed by large graphite impactors ($\approx$ 0.2 mm) and impactors consisting of submicron grains of graphite aggregated by electrostatic attraction into various-sized lumps. Raman characteristics of both are given below under graphite craters.

Two distinct morphologies were observed: (1) a very thin liner with peculiar linear ridges in the large crater (Fig. 2a) and (2) liners that are lumpy and common to the small craters (Fig. 3). Figure 2b shows a series of subparallel ridges that traverse the entire crater and rim; the ridges do not appear to extend beyond the crater. FESEM images (Figs. 2c, d) show that these ridges consist of impact altered carbon and small amounts of Al. Carbon spheres (0.002-0.018 mm dia) are common on the upturned rims and Al melt splatter covered by carbon was found on the upper portions of the steep walls. The entire crater is thinly covered by a liner of smooth, vitreous-like carbon (Fig. 2c). The small crater liners are lumpy and are evenly distributed along the crater bottoms and walls, but are thin and discontinuous along the rims (Fig. 3). Melted Al droplets were not evident on the surface of the liners.

Graphite Craters. These craters also contain large areas of shiny, melt-like carbon, although crater liners are less lumpy compared to submicron graphite craters.(Fig. 3). The Raman spectrum of crystalline graphite consists of a single band (below 2000 cm^{-1}) at 1580 cm^{-1}. Raman spectra of poorly crystallized graphite (PCG) and glassy or vitreous carbon have additional bands in this spectral region at 1360 and 1620 cm^{-1}. The intensity of the band at 1360 cm^{-1}, relative to the band at 1580 cm^{-1} (height and width), is taken to indicate the degree of disorder in PCG and vitreous carbon.

The Raman spectrum of prelaunched graphite is shown in Fig.11a together with three typical spectra obtained from graphite impacted craters in Al. The spectrum shown in Fig. 11b is that of

mostly crystalline graphite with some disordered carbon. This measurement was obtained only from the centers of the craters. The spectrum shown in Fig. 11c was also obtained primarily from material inside the craters, although it is commonly observed when the incident beam is focused on the wall of the crater or between the crater wall and the area towards the crater center. This spectrum is similar to that obtained for typical vitreous carbon and carbon from the Allende meteorite (ref. 18). The Raman spectrum shown in Fig. 11c is also found for PCG when it is heated in argon beyond 1200°C for up to 0.5 hrs. The spectrum in Fig. 11d is most often obtained from areas on the raised rim of the craters and areas outside the craters just beyond the rims. The spectrum is indicative of even greater disorder in PCG material. It is comparable to the spectrum obtained from carbon in the Murchison meteorite (ref. 18). Upon heat treating such carbon at 1200-1500°C, the Raman spectrum becomes similar to that shown in Fig. 11c (ref. 18).

The variations observed in the Raman spectra are continuous among those shown in Fig. 11 and suggest mixtures of various types of carbon. Moreover, the spectra shown are those most commonly obtained from given regions of large (> 0.04 mm dia) craters. The above observations are based on ≈ 50 measurements obtained at various positions inside and outside the craters. More extensive correlations may show differences in distributions of carbon types and may also be crater-size dependent.

Diamond Craters. Regardless of their size, diamond craters contain much thicker, continuous liners compared to the other experimental carbon impactor craters (Fig. 5). Initial observations indicate several characteristic features of carbon residue. Figure 5c shows melt-like stringers and a large melt droplet on the crater wall. SEM-EDS analysis indicates a weak Al signal; thus, we conclude that the melt liner and the droplet are carbon. This melt liner is covered by a thin layer of dusty carbon. Raman analyses show that the layer is a mixture of amorphous carbon and highly disordered PCG. The crater bottom consists of submicron grains and tiny "melt" spheres (Fig. 6). The spheres may be the amorphous and vitreous carbon in the Raman analyses.

Raman spectrum of natural diamond consists of a broad band at 1330 cm^{-1}. Raman spectra of diamond impact craters in Al are the same as those obtained for PCG and vitreous carbons (Fig. 11c) and are similar to spectra given by carbon in the Allende meteorite. In some of the spectra, there is an indication of a shoulder at 1330 cm^{-1} which could be due to diamond; the vitreous band at 1360 cm^{-1} is intense and may obscure this portion of the diamond band.

There is apparently some difference in the various carbon distributions in the large craters (> 0.1 mm) and small craters (< 0.1 mm). Raman spectra of highly disordered (amorphous) carbon were obtained from the raised rim of small craters but not from the center of the crater, whereas no spectrum was obtained from the raised rim of the large craters, although measurements could be obtained from the crater interiors (bottoms).

Fullerene Craters. The bottoms and walls of these craters are characterized by a splatter-like texture that consists of spheres and branch-like structures of dark red fullerenes (Fig. 7). LIMS, (ref. 9) and Raman analyses confirm the presence of molecular C_{60} and C_{70} (fullerenes). Small amounts of red-brown dusty ejecta are present around many of the craters.

Raman spectra from prelaunched fullerenes (fullerenes have Raman bands at ≈ 1450 and 1560 cm^{-1}) and impact residues from inside and around fullerene craters are the same, indicating that fullerenes remained intact on impact (Fig.12).

Phthalic Acid Craters. Figure 8 shows that the irregular-shaped craters contain featureless impactor in crater bottoms with concentric ridges of impactor material on the walls. LIMS analyses indicate that the bulk of the impactor residuum is mostly intact phthalic acid molecule with lessor amounts of lower mass fragmented molecules and a few unidentified higher mass molecules (Fig. 9).

Murchison Meteorite Craters. These craters have considerable amounts of retained impactor, some apparently intact impactor, and impact alteration features that are unique among those described in this work (Fig. 10). Crater bottoms commonly have melt beads that grade into peculiar sponge-like structures at the lower portions of the wall (Figs. 10b and c). The upper walls and rims have large amounts of irregular-shaped melted to partially melted impactor.

Analytical Results

Murchison Meteorite Impactor Residues. For the purpose of comparison and proper identification of PAHs previously reported using conventional wet chemistry coupled with gas chromatography/mass spectrometry, a separate non-impacted sample of Murchison meteorite was analyzed (Figure 13). The dominant masses of 128, 178, 192, 206 and 220 correspond to naphthalene, phenanthrene/anthracene, methyl phenanthrene, fluoranthrene/pyrene, C_{16} - alkylphenanthrene/C_{16}- alkylanthracene and C_{17}-alkylphenanthrene/C_{17}-alkylanthracene respectively, which is consistent with the PAH analyses of Murchison reported by other groups (refs. 19, 20). The upper spectrum in Fig. 13 represents a single shot spectrum and the lower spectrum represents an average of 100 shots.

The two impacted samples were than analyzed and compared to the non-impacted Murchison samples (Figures 14 a and b). Figure 14a represents a 100 shot averaged spectrum for the sample impacted at 4.8 km sec^{-1}. The dominant masses of 142, 178, and 220 correspond to methylnaphthalene, phenanthrene/anthracene and C_{17}-alkylphenanthrene/C_{17}-alkylanthracene, respectively. Masses 128, 192, 202, and 206 present in the non-impacted Murchison sample are not seen in the impacted sample. Two different sample discs of the 4.8 km sec^{-1} sample were analyzed and show good reproducibility of the spectrum (Fig. 14b).

Figure 15a represents a 100 shot averaged spectrum for the sample impacted at 5.9 km sec^{-1}. Masses 184, 202, 206, 220, and 234 correspond to C_{14}- alkylnaphthalene, fluoranthrene/pyrene, C_{16}-alkylphenanthrene/C_{16}-alkylanthracene, C_{17}-alkylphenanthrene/C_{17}-alkylanathracene and C_{18}-alkylphenanthrene/C_{18}-alkylanthracene. In this sample the lower masses 128, 142, and 178 are no longer present but the higher masses 184, 202, 206, 220 are at least, in part, preserved. This is consistent with what one might expect to see since the lower molecular weight PAHs would likely be the first to decompose/evaporate with the temperatures incurred at impact. There also appears to be an increase in alkylation compared to the non-impacted Murchison (Fig. 13) which would indicate that some of these PAHs were derived from more extensively heated precursors (probably due to impact) since the high extent of alkylation of PAHs has been attributed ot the thermal cracking of the "organic polymer" (ref. 21). Two different sample discs (Fig. 15b) of the 5.9 km sec^{-1} were also analyzed and show good reproducibility of the spectrum.

All three samples were scanned for higher mass compounds both in the porphyrin and fullerene ranges, but no masses were observed.

Figure 16 shows the bulk fluorescence for the non-impacted sample (16a), the 4.8 km sec^{-1} impacted sample (16b), and the 5.9 km sec^{-1} impacted sample (16c). For these samples, we have not yet attempted to analyze for the individual species which will require a mating of the LIF to liquid chromatography. The fluorescence for both the non-impacted and the impacted meteorite bulk samples are intense and similar which suggests that at least PAHs identified by L^2MS can survive impacts. The LIF has been able to detect C_{60} standards in the 10^{-8} to $2x10^{-5}$ g range (ref. 20), although none were found in these analyses.

DISCUSSION

Examination of the experimental residues of graphite and diamond show diverse morphological features and impact-induced modifications, which were not unexpected in view of their differences in density, porosity, structural characteristics, bonding characteristics, bond energies, etc. On the other hand, phthalic acid, fullerenes, and Murchison PAHs show somewhat unanticipated molecular survivability on impact. The following discussion addresses these issues and first-order questions raised in the Introduction.

Diamond and Graphite

The apparent total destruction of diamond at an impact velocity < 5.0 km sec^{-1} is somewhat surprising. We can assume from our other experiments and theoretical considerations (refs. 22, 23) that residue material did not necessarily experience peak pressures and temperatures during impact, otherwise molecules such as PAHs would have been destroyed. By analogy, the carbon (PCG) in the diamond-formed craters probably formed from diamond at less than peak pressures and temperatures which occur only at the initial projectile/target interface. Any recovered material experienced less stress than the initial interface. We do not know what these P-T conditions were during impact, but from (ref. 22) we know that for impact of soda-lime glasses into Cu at ≈ 5 km sec^{-1}, peak pressures were > 65 GPa and temperatures ≈ 3000° K. Other clues come from the carbon phase diagram (Fig. 17) of Bundy (ref. 24). The presence of PCG (graphite) and melt carbon (liquid) and the absence of diamond suggest a position on the diagram near the triple point or in the range of 4000° K and < 14 GPa. This position on the diagram is near the region of "fast reaction" of diamond to graphite (ref. 25). Alternatively, our assumption that liquid carbon formed and is represented by the vitreous carbon droplets and balls in Fig. 6 may be incorrect and these graphitic objects may have formed as small, spherulitic graphite spheres from the decomposition of diamond at much lower temperatures. In either case, the evidence suggests that the pressures on the trailing side of the diamond impactor were insufficient to allow diamond to remain stable in a high temperature regime during impact.

The possibility that intact diamond is buried under the residue surface cannot be precluded. The analytical techniques that we have used are surface analyzers (tens of nanometers to micrometers deep); intact diamond may exist below the surface levels that we analyzed. Raman analysis of the residue does not show a well-defined peak for diamond at 1330 cm^{-1} (although it may be obscured by other carbon signals or weak signals from buried diamond below the surface). The band shape may indicate that diamond is just below the surface and out-of-range for a sharp signal or, conversely, that any diamond present at the surface is either highly disordered diamond or mixed phases of disordered diamond and graphite. In any case, the hope of seeing intact diamond from meteoritic or interstellar sources in LDEF craters is remote.

Raman spectra indicate that intact, well-ordered graphite did survive impact, together with partially disordered graphite in the crater bottom centers. The degree of disorder increases away from the crater centers. This suggests that material found in the centers probably represents material that experienced the least amount of shock-induced damage. Impactor material outside of the craters, which shows the highest degree of disorder, was probably ejected early in the crater formation stages and was exposed to higher pressures and temperatures, in addition to having cooled more rapidly. In fact, all residues cooled exceedingly fast as the entire crater forming event probably took no longer than nano- to microsecs (refs. 22, 23), although cooling continued after the pressures dropped to the ground state. The cooling rate is unknown, but sufficiently high to prevent annealing/ordering to occur. Thus, the graphite that was disordered by very high temperatures was not annealed. Rims and the upper walls captured some of the late-stage ejecta and melt splash before the crater cavity formation was completed; this residue material is intermediate in the degree of disorder between that of the centers and the outside ejecta.

Phthalic acid and Murchison Meteorite

The two impacted Murchison samples both show preservation and destruction of some PAHs compared with the non-impacted Murchison sample. The differences in PAH compositions between the two impacted samples may be attributed to the well-known inhomogeneous distribution of organics within the whole meteorite (ref. 26). The samples taken for these impacts may also represent different parts of the meteorite. However, the

consistent absence of the low mass PAHs in all cases of both impactor residues and the very good reproducibility of the analyses coupled with an average of 100 analyses for each impactor residue where the low mass PAHs are missing, strongly suggest that the missing lower mass PAHs, which have lower boiling points (T_b K), vaporized on impact. The T_b K values for the missing PAHs are < 500, whereas T_b K for the surviving PAHs are > 600 (ref. 27) which could imply an upper, effective evaporation temperature limit sustained during impact for the surviving PAHs. Thus, it appears that at least some of the higher mass PAHs common in meteorites like Murchison, can survive hypervelocity impact under the experimental conditions presented here.

From the above, we have shown that some organic molecules can survive low hypervelocity impact into Al targets (phthalic acid at 4.2 km sec^{-1} and Murchison meteorite higher molecular weight PAHs at least up to 5.9 km sec^{-1}). Kinetic parameters from shock tube experiments with simple, low molecular weight organic compounds show that they can withstand shock temperatures up to 1500° K for a duration of ≤ 1 sec.; heavier, more complex aromatics may also survive at these temperatures and reaction times (ref. 23). As we have indicated above, peak pressures and temperatures are unknown for our experiments; however, they would certainly be sufficient to destroy all Murchison organic compounds if all of the kinetic energy of the impactor were available for impactor melting. Actually, much of an impactor's kinetic energy is probably partitioned into target heating, target excavation, and target/impactor ejection (ref. 28). In addition, an uneven distribution of shock energy through the impactor would possibly allow some portion of the impactor to experience temperatures under which some organic compounds could survive. Thus, from these considerations and from the results of our experiments, we expect to be able to find some surviving organic species in LDEF carbonaceous impactor residues, if indeed, any were present in the preimpact IDPs.

Fullerene Formation/Destruction Conditions

Since no fullerenes were found in the ppm range in carbonaceous impactor craters, we can assume that conditions were inappropriate for their formation. Our failure to make fullerenes by impact could be due to any number of reasons, e. g., nucleation/growth kinetics, improper temperatures and pressures, accompaning compositional interference, etc. Shock compression ("flying plate") experiments made under known P-T conditions suggest that fullerenes are stable up to 17 GPa (ref. 29). However, these experiments recorded the stability of fullerenes under more evenly distributed shock loading compared to those that arise from crater forming events where pressures and temperatures fall rapidly as crater formation proceeds. Even though these experiments are not directly analogous to crater forming events, they do establish that fullerenes are remarkably incompressible and remain unchanged to moderately high shock pressures. Future experiments may be designed to further address the issues of fullerene stability or formation on hypervelocity impact. The questions as to whether fullerenes pre-existed before impact on LDEF or were formed by impact remain unanswered.

Laser ionization mass spectroscopy techniques have been able to detect PAHs in meteorites on the sub ppm level (ref. 20)and ppb range (ref. 30). Other analyses of PAHs in the Murchison meteorite by similar L^2MS techniques suggest that cosmic abundances of hydrogen in circumstellar or interstellar environments may have precluded the synthesis of fullerenes, but not the production of PAHs (ref. 30). Recently, a carbonaceous residue from an LDEF crater was analyzed by LIMS and Raman methods and the presence of fullerenes was confirmed (ref. 9). Very low concentration levels of fullerenes in other LDEF craters or in meteorites could be identified by using the LIF system which could help address the issues of fullerene formation in space environments.

CONCLUSIONS

Intact remnants of diamond impactors were not found. Diamond was converted during impact (4.8 km sec^{-1}) to various disordered forms of graphite (PCG). Diamond crater morphology is unique among carbon impactors in having thick residue liners. Graphite impactor residue, formed at impact velocities up to 5.9 km sec^{-1}, shows some intact, well-ordered graphite in the residue of crater bottom centers; the degree of disorder increases outward to the ejecta.

Fullerenes were not formed on impact from carbon-bearing precursors (diamond, graphite, phthalic acid, Murchison particles). Moreover, fullerene impactors mostly remained as fullerenes after impact at 5.9 km sec^{-1}.

Phthalic acid crystals were destroyed on impact, although much of the molecules remained intact at the impact velocity of 4.2 km sec^{-1}.

Murchison meteorite residues in the crater bottoms have an unusual, sponge-like morphology which may be the result of the precursor's abundance of water-bearing, layer-lattice silicates. This type of morphology may prove to be useful in distinguishing between hydrous and anhydrous particles that impacted at velocities $\leq$ 6 km sec^{-1}.

Some PAHs (mostly the higher mass species) in the impacted Murchison meteorite samples survived impact. From theoretical considerations and our experimental results, we expect to find some surviving carbonaceous impactor organic compounds in LDEF craters that formed up to $\approx$ 10 km sec^{-1} impact velocity.

LIF detection is not limited to bulk analyses such as those that we carried out, but can be used as an on-column detector for HPLC, microbore HPLC and open tubular liquid chromatography. The great mass sensitivity of LIF coupled with these systems should permit the analyses of trace quantities of organic compounds and help to differentiate among other carbonaceous materials such as fullerenes and thus determine whether fullerenes occur naturally in cometary and asteroidal (IDPs) samples.

REFERENCES

1. See, T.; Allbrooks M.; Atkinson D.; Simon C.; and Zolensky M.: Meteoroid and debris impact features documented on the Long Duration Exposure Facility a preliminary study. *Planet. Sci Branch Publ.* # **73** (JSC # **24608**), 1990.

2. Hörz, F.; Bernhard, R. P.; Warren, J.; See, T.; Brownlee, D. E.; Laurance M. R.; Messenger, S.; and Peterson, R. B.: Preliminary analysis of LDEF instrument A0187-1 "Chemistry of micrometeoroids experiment". *First LDEF Sym. NASA* **CP-3134,** 487-499, 1992.

3. Bunch, T. E.; Radicati di Brozolo, F.; Fleming, R. H.; Harris, D. W.; Brownlee, D. E.; and Reilly, T.: LDEF impact craters formed by carbon-rich impactors: A preliminary report. *First LDEF Sym. NASA* **CP-3134**, 549-564, 1992.

4. Peterson, E.; Hörz, F.; Haynes, G.; and See, T.: Modification of amino acids at shock pressures of 3 to 30 GPa. *Meteoritics* **26**, 384,1991.

5. Lewis, R. S.; Tang, M.; Wacker, J. F.; Anders, E.; and Steel. E.: Interstellar diamonds in meteorites. *Nature* **326**, 160-162, 1987.

6. Allamandola, L. J.; Sandford, S. A.; and Tielens, A. G. G. M.: Interstellar "diamonds" in dense molecular clouds. *Nature* 1992.

7. Allamandola, L. J.; Sanford, S. A.; and Wopenka, B.: Interstellar polycyclic aromatic hydrocarbons and carbon in interplanetary dust particles and meteorites. *Science* **237**, 56-59, 1987.

8. Langevin, Y.; Kissel, J.; Bertaux, J-L.; and Chassefiére E.: First statistical analysis of 5000 mass spectra of cometary grains obtained by PUMA 1 (Vega 1) and PIA (Giotto) impact ionization mass spectrometers in the compressed modes. *Astron. Astrophys.* **187**, 761-766, 1987.

9. Radicati di Brozolo, F.; Fleming, R. H.; and Bunch, T. E.: Observation of fullerenes in an LDEF impact crater. *Science* in press, 1992.

10. Chen, R.F.; Becker, L.; Bada, J.L.: Detection of C_{60} using Laser-Induced Fluorescence. *J. of Amer. Chem Soc.* 1992.

11. Odom, R. W.; and Schueler, B. W.: Laser microprobe mass spectrometry: Ion and neutral analysis. in *Lasers and Mass Spectrometry*, D. M. Lubman ed. Oxford University Press, 103, 1990.

12. Krätschmer, W.; Lamb, L.D.; Fostivopoulos, K.; and Huffman, D. R.: Solid C_{60}: A new form of carbon. *Nature*, **347**, 354, 1990.

13. Hahn, J.H.; Zennobi, R.; Zare, R.N.: Subfemtomole quantitation of molecular absorbates by two-step laser mass spectrometry. *J.Am, Chem.Soc.* **109**, 2842-2843, 1987.

14. Engelke, F.; Hahn, J.H.; Henke; W., Zare; R.N.: Determination of phenythiohydrandion-amino acids by two-step laser desorption/multiphoton ionization. *Anal. Chem.* **59**, 909-912, 1991.

15. Hillenkamp; F.; Karas, M.; Beavis; R.C.; Chait; B.T.: Matrix-assisted laser desorption/ionization mass spectrometry of biopolymolecules. *Anal. Chem.* **63**, 24-37, 1991.

16. Zare, R.N.: Laser chemical analysis. *Science* **226**, 298-303, 1984.

17. Chen, R.F.and Bada, J.L.: A laser-based fluorometry system for investigations of seawater and porewater fluorescence. *Mar. Chem.* **31**, 219-230, 1990.

18. Macklin, J.; Brownlee, D. E.; Chang. S.; and Bunch, T. E.: Micro-Raman spectroscopic measurement of carbon in meteorites and interplanetary dust particles. *Microbeam -87*, 211-212, 1987.

19. Oro, J. et al.: Amino acids, aliphatic and aromatic hydrocarbons in the Murchison meteorite. *Nature* **230**, 105-106, 1971.

20. Hahn; J.H.; Zenobi, R.; Bada; J.L., Zare; R.N.: Application of two-step laser mass spectrometry to cosmochemistry: Direct analysis of meteorites. *Science* **239**, 1523-1525, 1988.

21. See Tissot, B.P. and Welte, D.H.: *Petroleum Formation and Occurrence*. Springer-Verlag, Berlin, 1984 for a comprehensive review of pyrolysis of aromatic compounds.

22. Hörz, F.; Fechtig, H.; and Janicke, J.: Morphology and chemistry of projectile residue in small experimental impact craters. *Proc. 14th Lunar Planet. Sci. Conf. Part 1, J. Geophy. Res.* **88**, B353-B363, 1983

23. Chyba, C. F.; Thomas, P. J.; Brookshaw, L.; and Sagan, C.: Cometary delivery of organic molecules to the early Earth. *Science* **249**, 366-373, 1990.

24. Bundy, F. P.: *Physica* A**156**, 169-178. 1989.

25. Regueiro, M. N.; Monceau, P.; and Hodeau, J-L.: Crushing C_{60} to diamond at room temperature. *Nature* **355**, 237-239, 1992.

26. See Nagy, B., *Carbonaceous Meteorites*. Elsevier, Amsterdam, 1975 for a comprehensive review of this early research.

27. White. C. M.: Predictions of the boiling point, heat of vaporization, and vapor pressure at various temperatures for PAHs. *J. Chem. Eng. Data* **1986**, 31, 198-203, 1986.

28. O'Keefe, J. D. and Ahrens, T. J.: in *Geololgical Implications of Impacts of Large Asteroids and Comets on the Earth,* L.Silver and P. Schultz, eds. *Geol. Soc. Am.* **SP-190.** 103-120, 1982.

29. Yoo, C. S. and Nellis, W. J.: Phase transformations in carbon fullerenes at high shock pressures. *Science*, **254,** 1489-1491, 1991.

30. De Vries, M.S.; Wendt, H.R.; Hunziker, H.; Peterson, E.; and Chang, S.: Search for high molecular weight polycyclic aromatic hydrocarbons and fullerenes in carbonaceous meteorites. *Lunar and Planetary Sci. XXII*, 315-316 1991.

ACKNOWLEDGEMENTS

We thank B. Langedyk, W. Logsdon, and J. Vongrey for their assistance during the impact experiments and the NASA OSSA Exobiology 199-52-12 and OAST 506-48 Programs for partially supporting this work. F. R di B and RHF acknowledge support from NASA SBIR Contract NAS2-13178. We also thank Sherwood Chang and Fred Hörz for critical reviews and helpful suggestions.

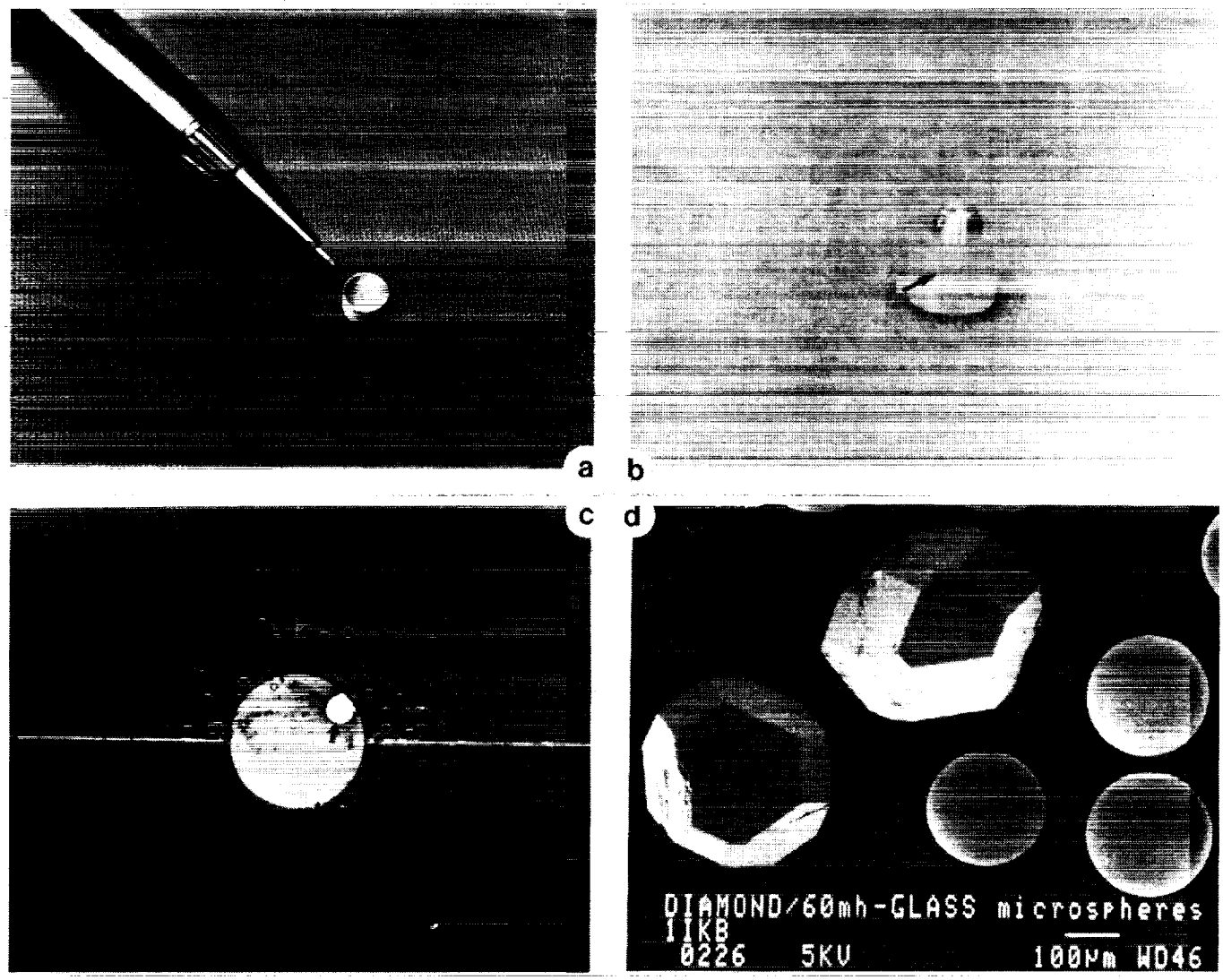

Figure 1. (a) Particle carrier for cluster launches. (b) Carrier with lid set in a plastic sabot. (c) Witness plate showing alignment test pattern of craters produced by boron nitride projectiles. Hole in the center (2.5 cm in dia; covered with mylar film) is the escape hole for the carrier which made the hole in the mylar covering (NE quadrant). Smaller holes in the film are from passage of projectiles. (d) Example of diamond projectiles.

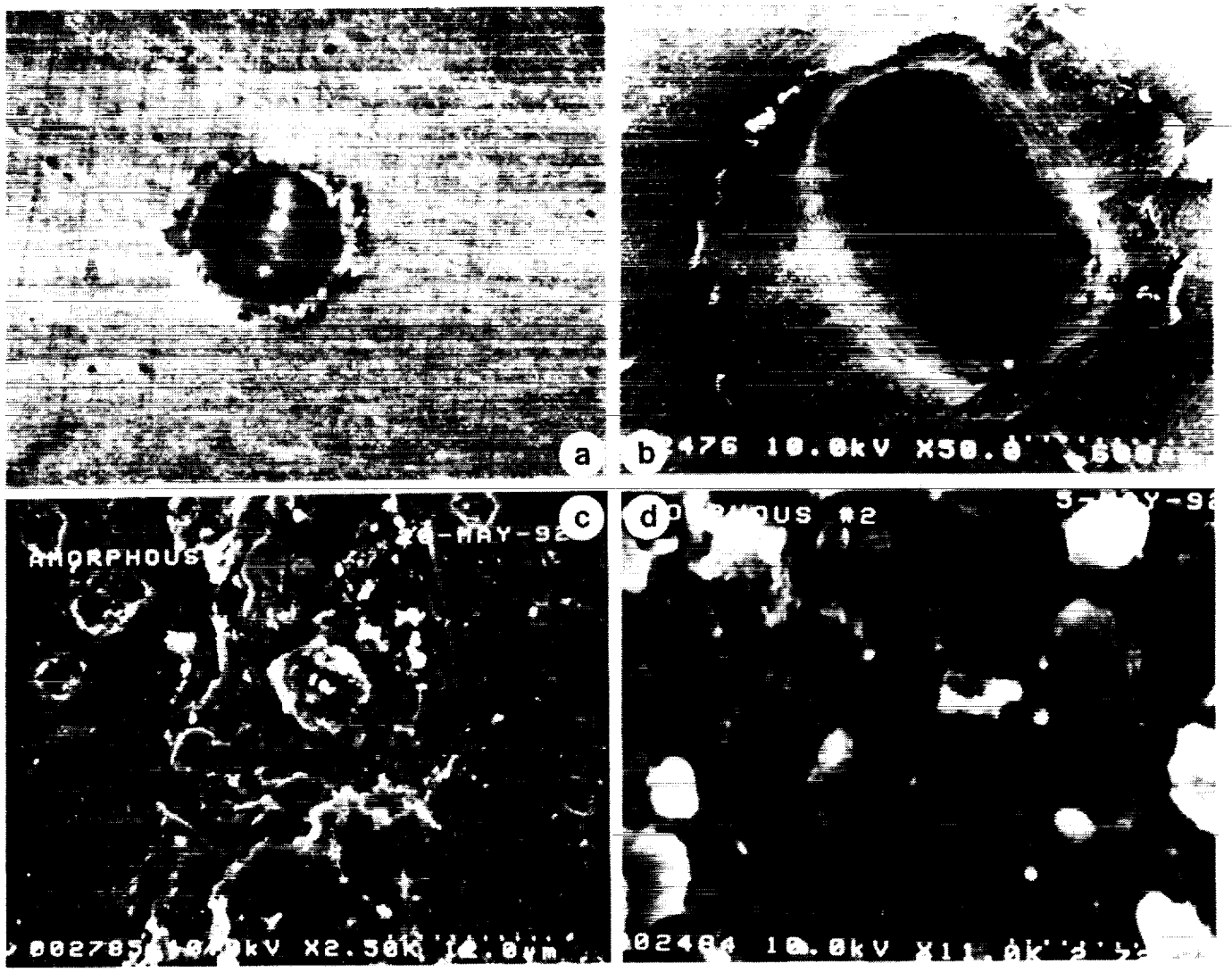

Figure 2. Large submicron graphite impactor craters. (a) Very large crater made from a statically clumped graphite impactor ball. Note the much smaller craters. Scale bar = 0.5 mm. (b) FESEM image of crater in a. Large arrow points to subparallel ejecta ridges. Small carbon melt spheres can be seen on the rim (small arrows). Scale for all FESEM images are given in the lower right hand corner. (c) Enlargement of ejecta ridge (center) on the carbon melt liner. (d) Enlarged view of the ejecta ridge material. Bright areas may be melted Al.

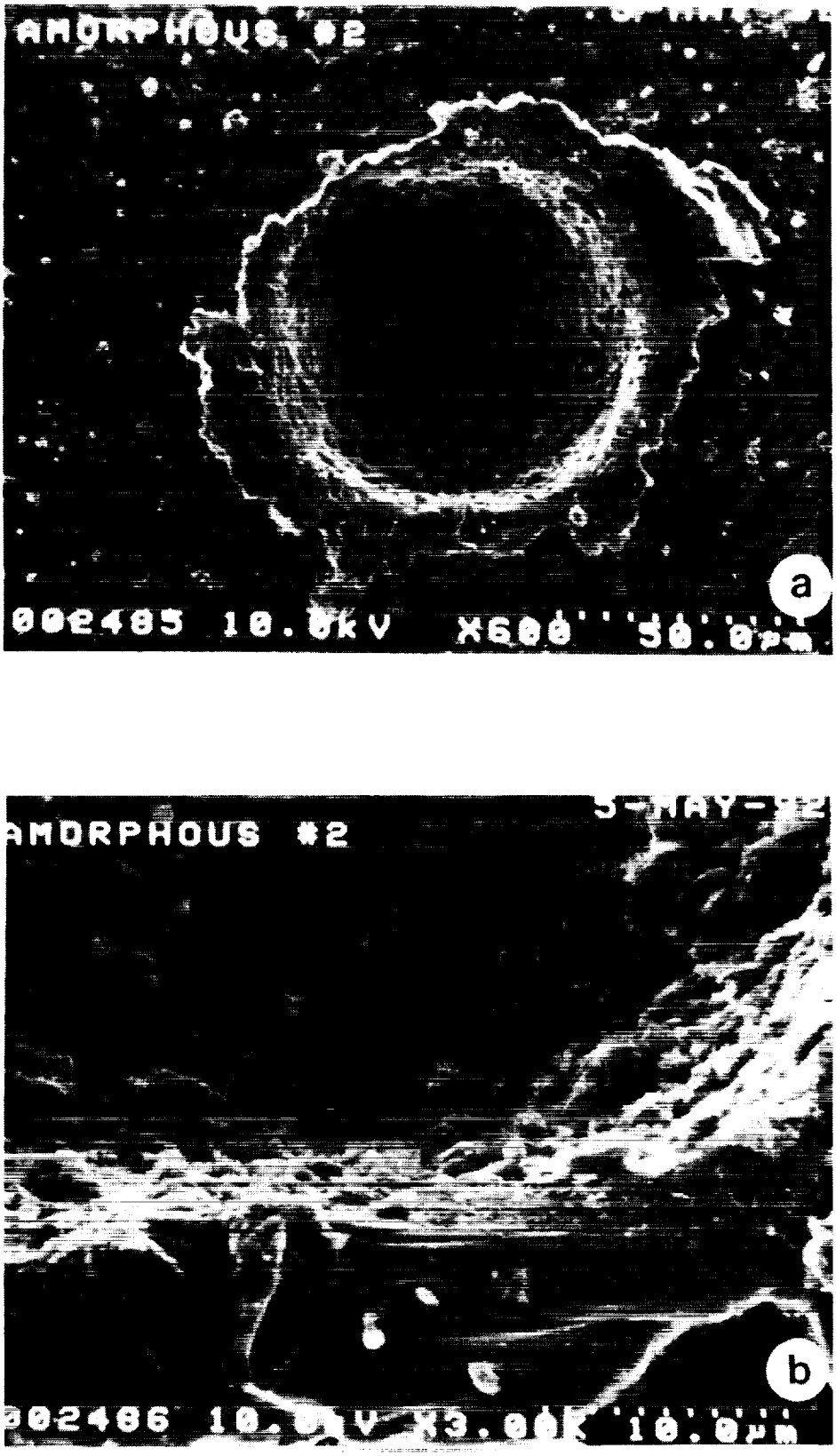

Figure 3. Small submicron graphite impactor craters. (a) Typical crater. (b) Image of impactor residue on the crater bottom (top), the wall (center), and rim (bottom).

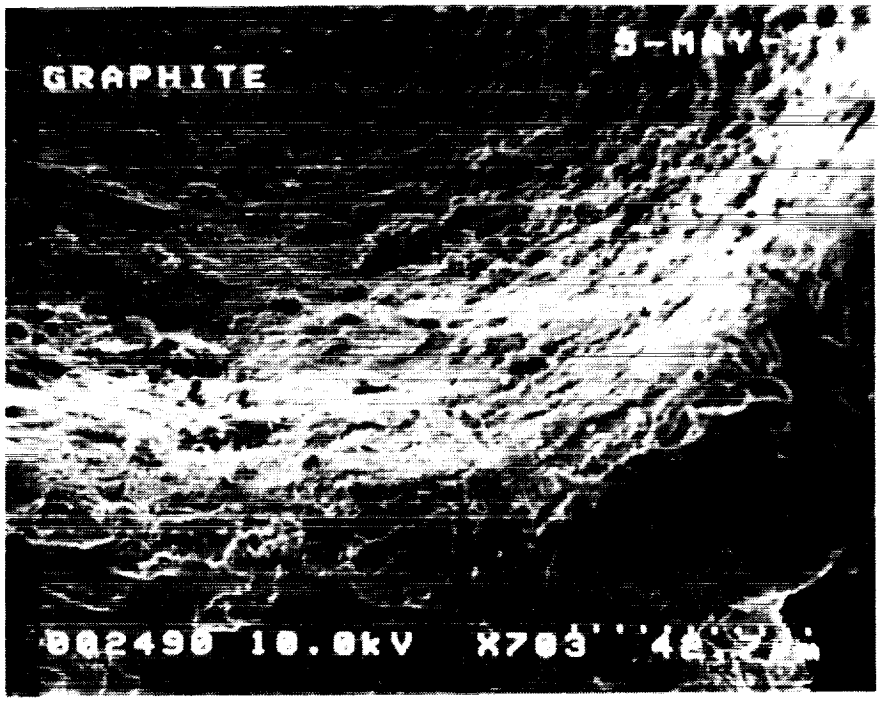

Figure 4. Coarse graphite impactor craters. (a) Typical crater. (b) Image of impactor residue on the bottom, wall, and rim.

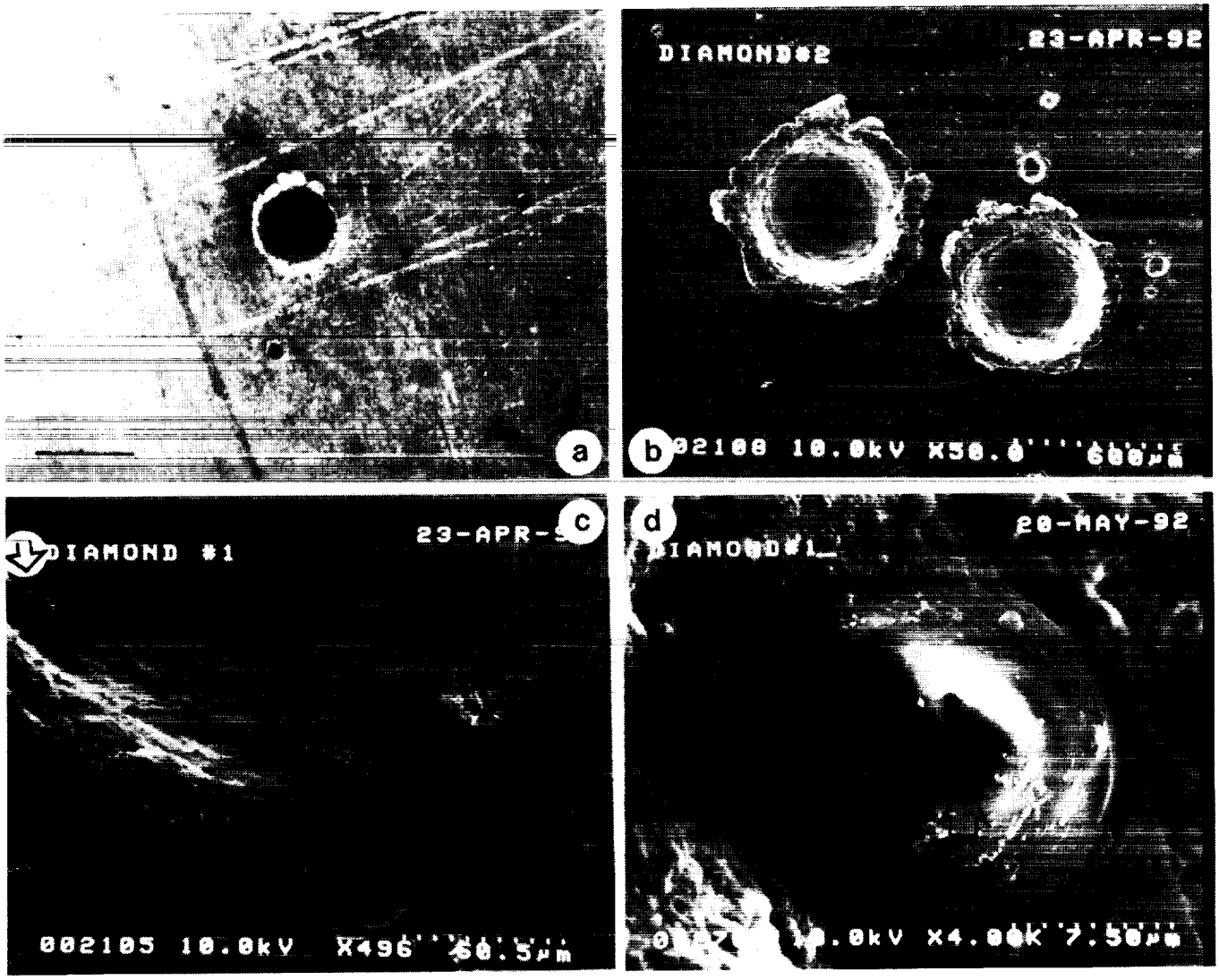

Figure 5. Diamond impactor craters. (a) Typical crater; note the black interiors. Scale = 0.5 mm. Oblique lighting, photomicrograph. (b) FESEM image; note darkened rims from carbon ejecta. (c) Image of impactor residue on bottom, wall, and rim. Note carbon melt droplet (arrow). (d) Close-up of droplet; arrow indicates a depression which may be due to shrinkage on cooling.

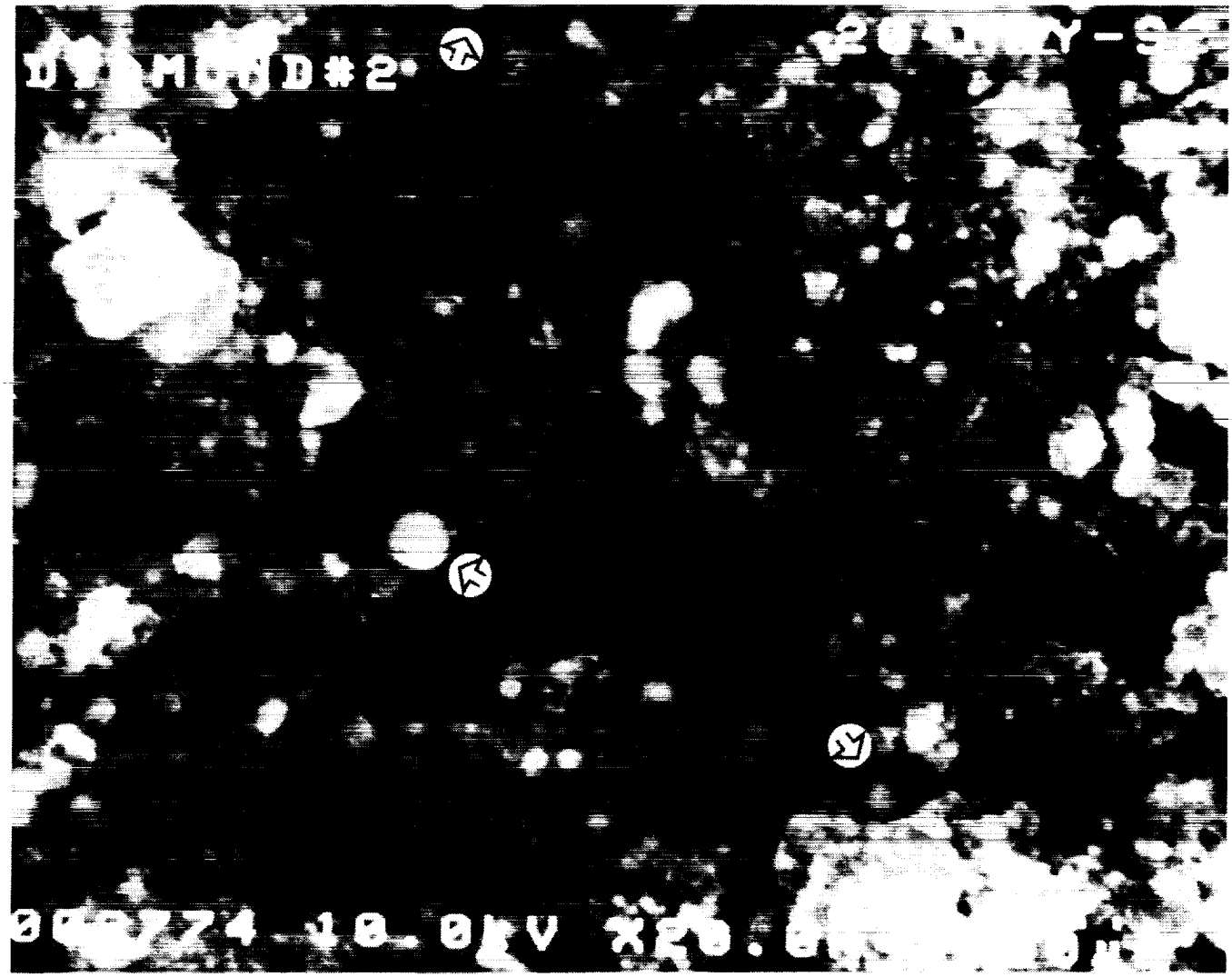

Figure 6. Enlarged image characteristics of diamond impactor residue. Arrows point to carbon melt balls (< 0.001 mm dia.) which, from Raman spectra, may be vitreous carbon; the other material is probably highly disordered graphite (PCG).

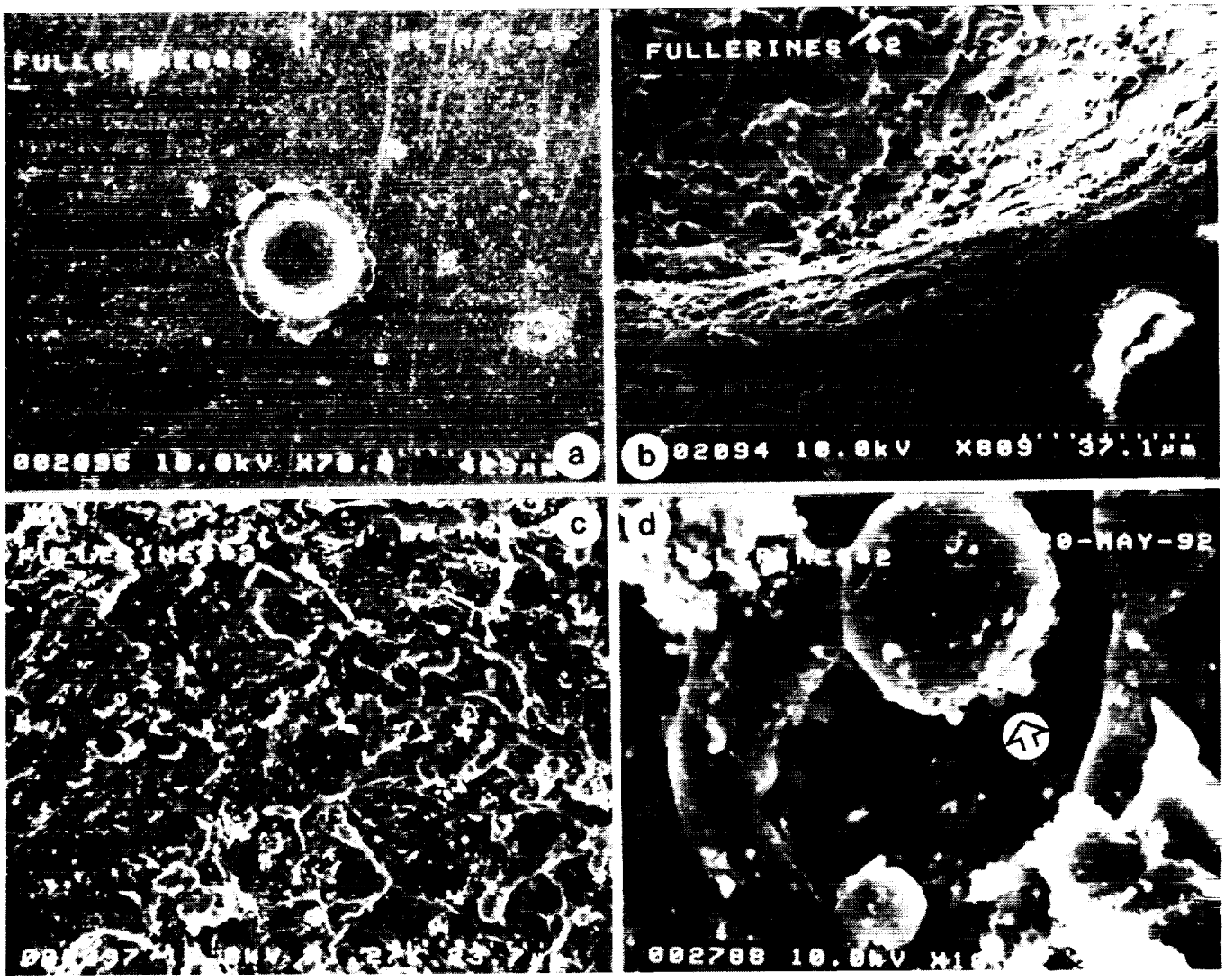

Figure 7. Fullerene impactor craters. (a) Typical crater. (b) Image of impactor residue on the bottom, wall, and rim. (c) Melt splatter features on the bottom and lower wall (turn image 180° to get a better perspective). (d) High resolution of material in c (arrow points to a 0.006 mm melt ball with attached rounded material (submicron).

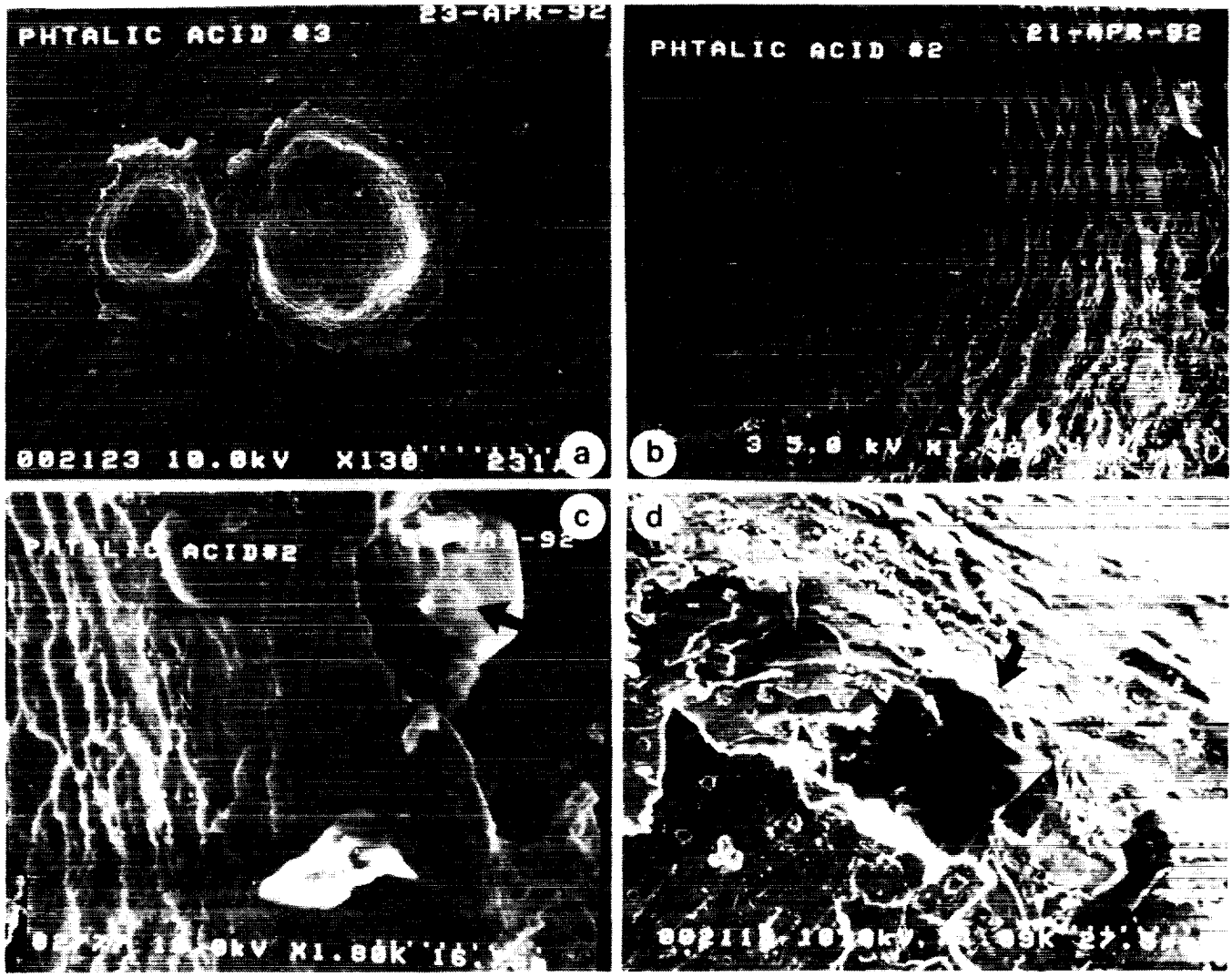

Figure 8. Phthalic acid impactor craters. (a) Typical craters showing irregular crater outlines. (b) Image of the residue on the bottom (left), lower wall (center), and upper wall (right). (c) Image showing top of rim and a partially melted impactor grain (arrow) that is outside of the crater and underneath the rim, possibly arising from ejection from a nearby crater. (d) Top of a rim; arrow points to a cluster of dipyramidal crystals of unknown composition.

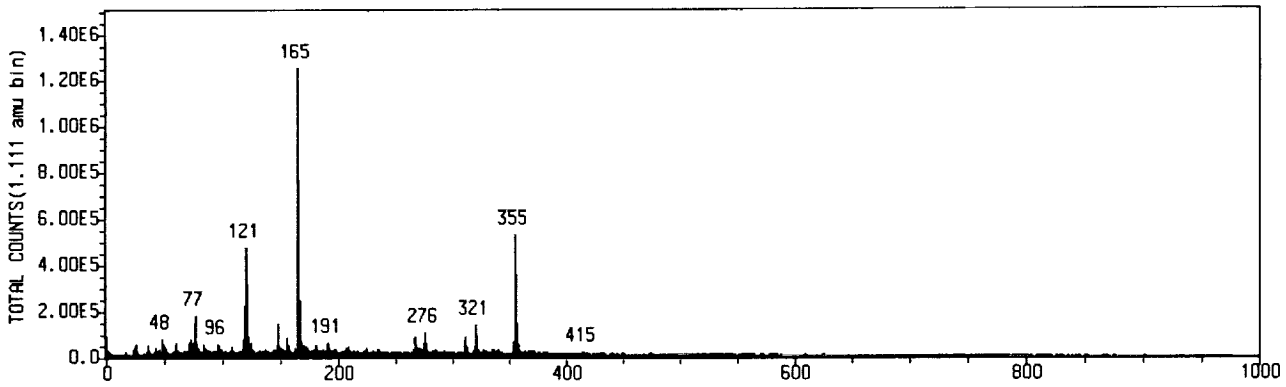

Figure 9. LIMS spectrum showing negative ion phthalic acid (mass 165), a phthalic acid molecular fragment (minus a carboxyl) at mass 121, and other unidentified masses.

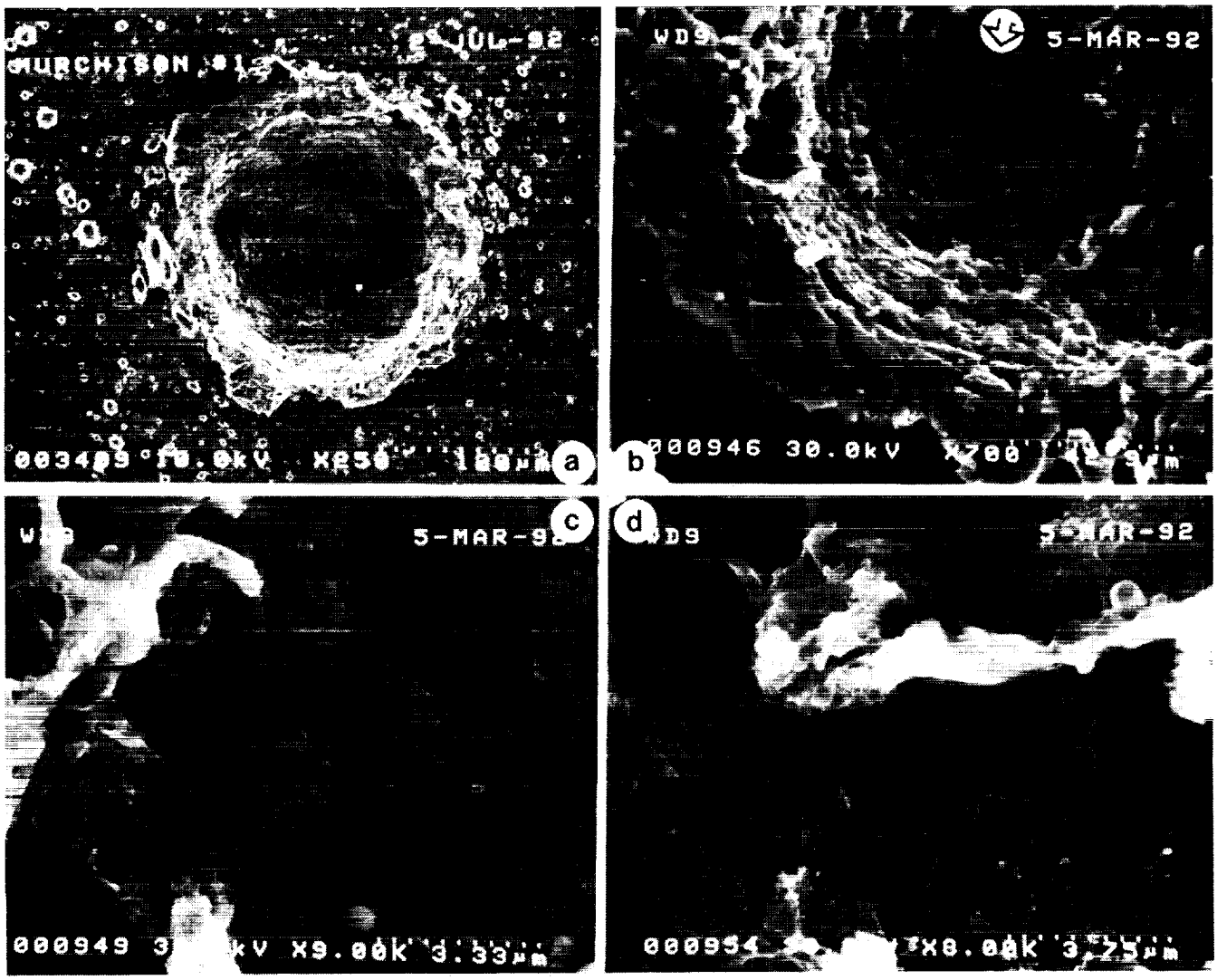

Figure 10. Murchison meteorite impactor craters. (a) Typical craters. (b) Image showing the residue on the bottom, wall, and rim (arrow refers to a melt blob in the bottom). (c, d) Close-up views of peculiar sponge-like melt features in the crater bottoms and walls.

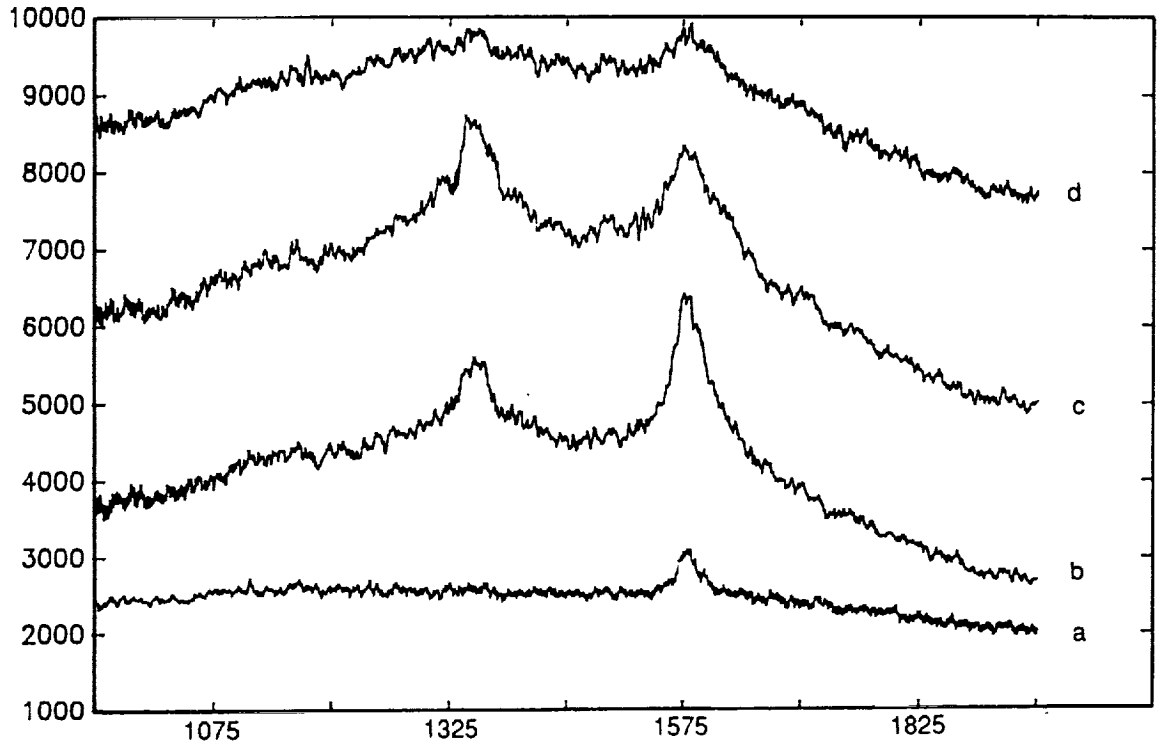

Figure 11. Typical Raman spectra of prelaunched graphite and impactor residues. (a) Precursor graphite. (b) Spectrum from crater centers. (c) Spectrum from crater walls to near the centers. (d) Spectrum from raised rim and outside ejecta.

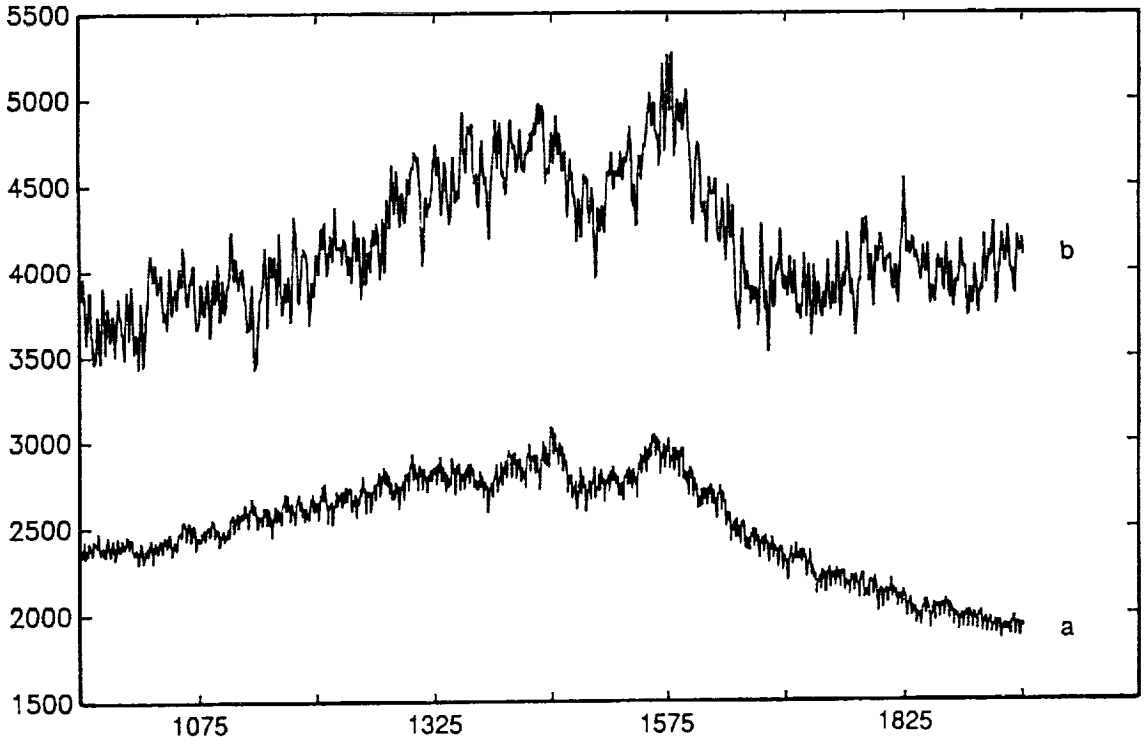

Figure 12. Typical Raman spectra of (a) precursor fullerenes and (b) fullerene impact crater residue.

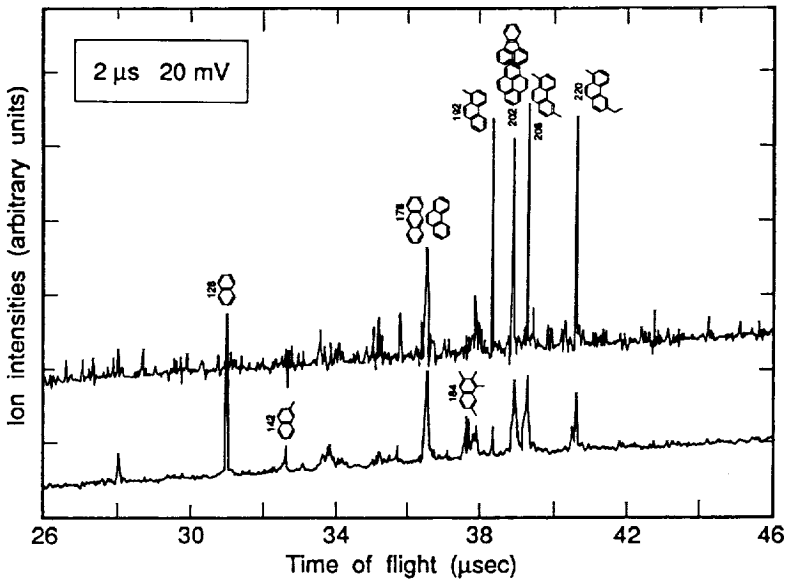

Figure 13. Laser desorption/multiphoton ionization TOF mass spectrum of non-impacted Murchison meteorite. Possible mass identification are: 128, naphthalene; 178, phenanthrene/anthracene; 192, methylphenanthrene; 202, fluoranthrene/pyrene; 206, C_{16}-alkylphenanthrene/C_{16}-alkylanthracene and 220,C_{17}-alkylphenanthrene/C_{17}-alkylanthracene. (a) Represents a single shot spectrum. (b) An average of 100 shots.

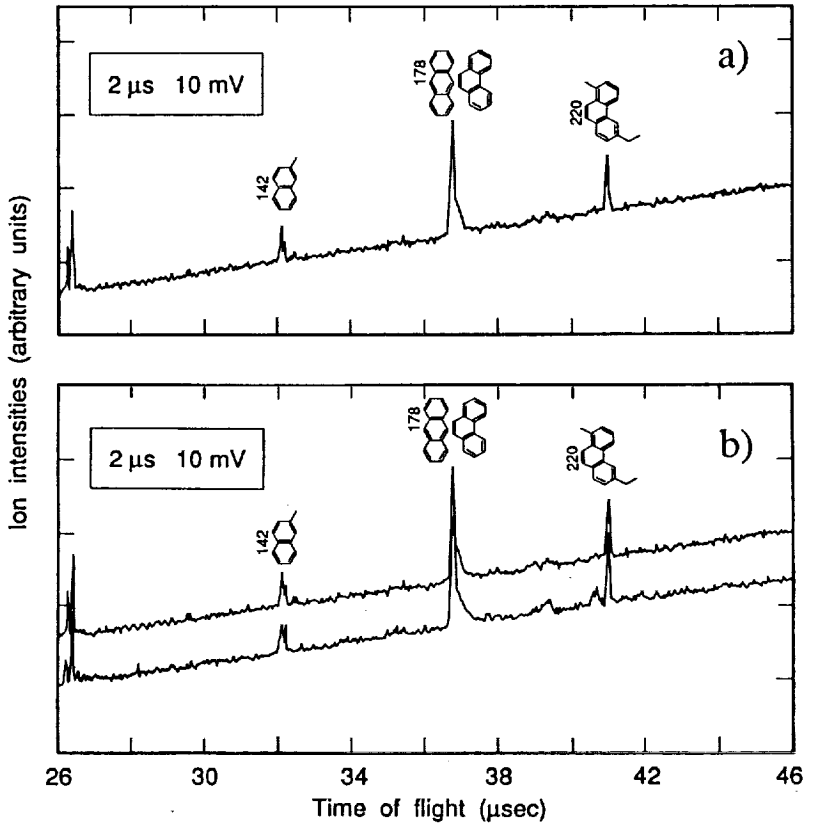

Figure 14. (a) 100 shot averaged spectrum for the sample impacted at 4.8 km sec^{-1}. Possible mass identification are: 142, methylnaphthalene; 178, phenanthrene/anthracene and 220, C_{17}-alkylphenanthrene/C_{17}-alkylanthracene. (b) Two different sample disks that show good reproducibility.

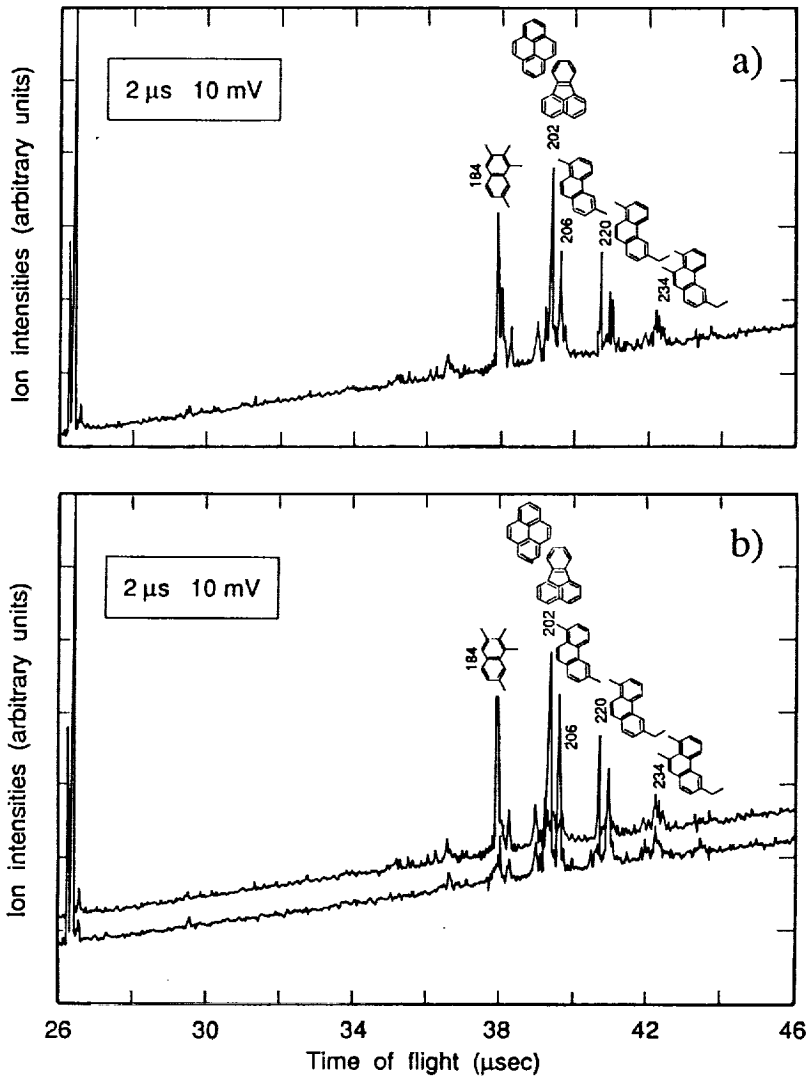

Figure 15. (a)100 shot averaged spectrum for the sample impacted at 5.9 km sec^{-1}. Possible mass identifications are: 184, C_{14}-alkylnaphthalene; 202, fluoranthene/pyrene; 206, C_{16}-alkylphenanthrene/C_{16}-alkylanthracene; 220, C_{17}- (b) Two different sample disks that show good reproducibility.

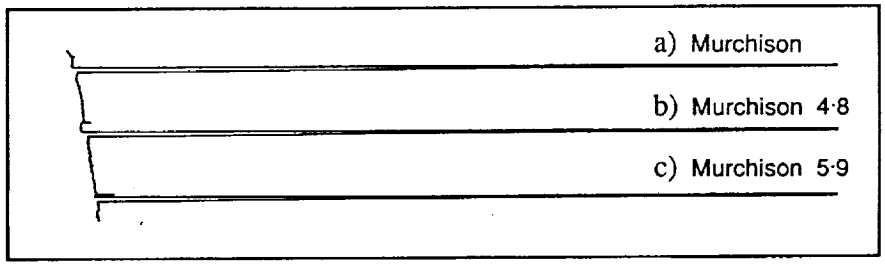

Figure 16. Bulk fluorescence using LIF for: (a) the non-impacted Murchison sample, (b) the 4.8 km sec^{-1} impacted sample, and (c) the 5.9 km sec^{-1} impacted sample.

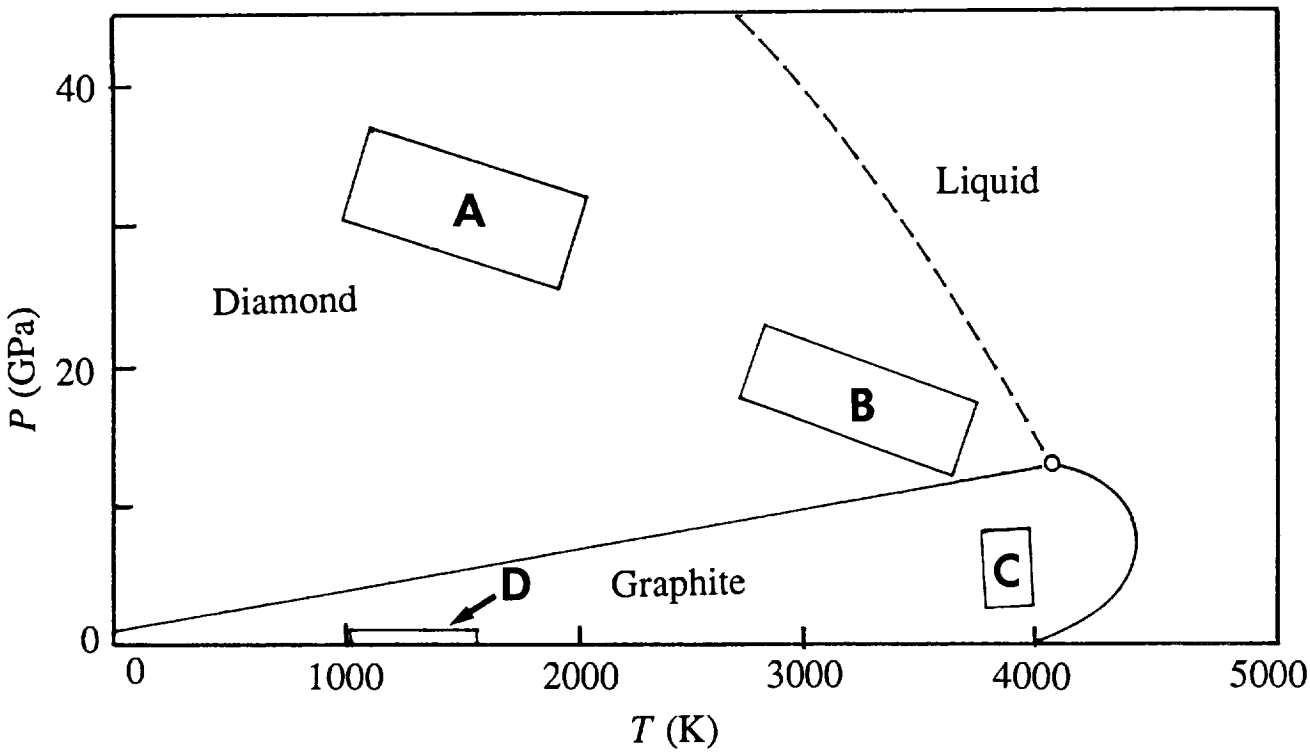

Figure 17. A portion of the carbon phase diagram (ref. 22). Field A is the region of shock conversion of graphite to diamond; field B is the region of "fast reaction", graphite to diamond; field C is the region of "fast reaction" diamond to graphite; field D is region of vapor deposited diamond films (ref. 25). The presence of both graphite and melt-droplet carbon (liquid carbon) and the absence of diamond in the diamond crater residue suggest that an area near the triple point in the diagram (liquid-diamond-graphite) was reached during impact for these products, but was below the diamond stability field, i. e., below a pressure of ≈ 14 GPa at 4000°K.